https://doi.org/10.5194/egusphere-2025-3661
Preprint. Discussion started: 14 August 2025

Features Investigates of the geospace storm over China During May 10–12, 2024

Tao Xu[1], Yaya Liu[1], Leonid Chernogor [1,2], Zhejun Jin[1], Mykyta Shevelev[2], Yevhen Zhdanko[2], Yu Zheng[1,*]

[1]College of Electronic and Information Engineering, Qingdao University, 308 Ningxia Road, Qingdao 266071, China; zhengyu@qdu.edu.cn (Y.Zh.) ; xutao55@qdu.edu.cn (T.X.); liuyaya@qdu.edu.cn (Y.L.); zhejunjin@qdu.edu.cn (Zh.J.)
[2]V. N. Karazin Kharkiv National University, Svobody square, 4, 61022, Kharkiv, Ukraine; leonid.f.chernogor@gmail.com (L.Ch.); mykyta.b.shevelev@gmail.com (M.Sh.); eugenezhd@gmail.com (Ye.Zh.)

Corresponding author:Yu Zheng, zhengyu@qdu.edu.cn

Abstract. This study investigates the characteristics of geomagnetic and ionospheric disturbances over China associated with the intense geospace storm that occurred during May 10–12, 2024. Observations were conducted using data from nine Intermagnet observatories, four ionosondes, and multiple satellites from the GNSS. To examine the quasi-periodic temporal variations of magnetic field components, this study introduces systems spectral analysis exclusively. The analysis reveals that the geospace storm, classified as a severe event, was accompanied by both intense geomagnetic perturbations and significant negative ionospheric storms. During the geomagnetic storm, the peak-to-peak amplitude of variations in the X-, Y-, and Z-components reached 550–800 nT, 166–422 nT, and 100–412 nT, respectively. The duration of the geomagnetic storm was approximately 40–60 h. The fluctuation spectrum of the geomagnetic field predominantly featured components with periods of 200 min and 90 min. During the negative ionospheric storm, which lasted around 50 h, foF2 values decreased by 2–3 times, while electron density values decreased by 4–9 times. At the same time, hmF2 values increased by 200–300 km. Other ionogram parameters exhibited minor changes. Total electron content values during the storm decreased by 30–40 TECU during the day (by 2–3 times) and by 10 TECU at night (by 2 times). The causes leading to the negative ionospheric storm was primarily driven by the penetration of magnetospheric electric fields into the ionosphere, the enhancement of plasma convection, disturbances in the thermospheric chemical composition, the intensification of thermospheric winds, and plasma transport processes occurring in both vertical and horizontal directions.

1 Introduction

Geospace storm is synergistically interacting storms occurring in the magnetosphere, ionosphere, thermosphere, and geophysical fields (magnetic, electric, baric, and thermal). The cause of geospace storms is solar storms, which induce significant disturbances in all subsystems of the Sun–interplanetary medium–magnetosphere–ionosphere–atmosphere–Earth (internal shells) system (Chernogor,2003,2021,2025). Magnetic, ionospheric, and atmospheric storms substantially affect radio wave propagation across all frequency ranges, as well as the operation of systems such as radio navigation, telecommunications, radar, remote sensing, and radio astronomy. This is due to the reliance of these systems on atmospheric, ionospheric, and magnetospheric radio channels (Wang, Feng, & Ma,2020).

As is known, the neutral atmosphere extends up to 55–90 km, depending on the time of day, with the ionosphere situated above it. The upper boundary of the ionosphere is conventionally defined at an altitude of approximately 1500 km. In contrast, the Earth's magnetosphere extends to about 10 Earth radii (~64,000 km) on the dayside. Geostationary satellites, which orbit at altitudes near 36,000 km, are thus situated well within the magnetospheric region. The magnetosphere, ionosphere, and atmosphere, along with associated geophysical fields, are seldom in a truly quiescent state (Shi et al.,2023). They are continuously influenced by energy fluxes originating from both the upper and lower atmospheric regions. The most significant impacts on these subsystems and fields arise from powerful transient processes on the Sun, commonly referred to as solar storms. Solar storms are accompanied by solar flares, the generation of solar cosmic rays, coronal mass ejections (CMEs), high-speed streams from coronal holes, and compression regions (CIRs).

The solar storm of May 8, 2024, triggered the most intense geospace disturbance recorded in the past two decades, with geomagnetic activity persisting from May 10 to May 15, 2024. Numerous studies have focused on the impacts of this extraordinary event. The energetics of the main physical processes within the Sun–interplanetary medium–magnetosphere–ionosphere–atmosphere–lithosphere system during May 8–12, 2024, were assessed by the author of (Chernogor,2025), who quantitatively substantiated the uniqueness of the storm. Detailed descriptions of the solar storm parameters and interplanetary medium disturbances are provided in (Hayakawa et al.,2025; Hajra et al.,2024; Kwak et al.,2024; Rodkin et al.,2024; Wang R.et al.,2024; Wang S.et al.,2019; Zhao & Le,2025; Vichare & Bagiya,2024; Fu et al.,2025). The paper (Pierrard et al.,2025) is devoted to the effects of the storm of May 11, 2024 in the Earth's radiation belts. The thermospheric effects during the geomagnetic storm of May 10–12, 2024 are the subject of (Evans et al.,2025; Mlynczak et al.,2024). The authors discussed the anomalous ionization of the Nocturnal E region during the storm on May 10–12, 2024. The effects of a super fountain caused by the extreme storm on May 10–12, 2024 are studied (Resende et al.,2024; Thampi et al.,2024). The authors studied the possibility of variations in quasi-periodic traveling ionospheric disturbances during the night of May 13, 2024, against the background of the recovery phase of a magnetic superstorm. The speed of disturbances was 300–650 m/s, and the period was close to 1 h (Zhang K.et al.,2025) .

The features of ionospheric storms at different latitudes have been analyzed in various studies. The effects of the storm in the ionosphere, as well as in the plasmasphere over the USA, Europe, and Southeast Asia are described (Pierrard et al.,2025). The authors have described the global ionospheric response to the solar storm (Li et al.,2024; Bojilova et al.,2024; Paul et al.,2025). The relationship between ionospheric and thermospheric processes in the Eastern Hemisphere during the negative ionospheric storm in the Northern Hemisphere and the positive ionospheric storm in the Southern Hemisphere in May 2024 was explored (Li et al.,2024). High-latitude ionospheric storm features have been examined (Chernyshov et al.,2025; Jin et al.,2025; Themens et al.,2024; Wang et al.,2024). Ionospheric effects of the storm at mid-latitudes have been described in papers (Jin et al.,2025; Bojilova,2024; Aa et al.,2024a; Carmo et al.,2024; Foster et al.,2024).Potential mechanisms of the super storm are discussed by the authors of (Tulasi Ram et al.,2024). A significant number of papers focus on the ionospheric response to the solar storm at low latitudes (Jain et al.,2025; Gonzalez - Esparza et al.,2024; Myint et al.,2025; Nayak et al.,2025; Singh et al.,2024). Particular attention has been given to the effects within the equatorial ionization anomaly (EIA) region (Nayak et al.,2025; Aa et al.,2024b; Huang et al.,2024; Karan et al.,2024; Rout et al.,2025). It has been shown that during the storm, the EIA region shifted from the equator up to latitudes of 35°N and 35°S.

This study specifically examine the ionospheric responses to the storm over the East Asian region.Multi-instrumental observations of the ionospheric response to the storm were conducted by (Guo et al.,2024), who described longitudinal differences in ionospheric disturbances. The negative ionospheric storm in the Chinese region began after the SSC on May 10, 2024, and continued throughout the main phase and the beginning of the recovery phase of the magnetic storm on May 11, 2024. During the recovery phase on May 12, 2024, the sign of TEC disturbances changed. More precise modeling of processes in various regions during May 10–12, 2024, storm is required. The authors of (Huang et al.,2024) also analyzed the results of multi-instrumental observations and found that the nighttime increase in total electron content (TEC) moved westward at a speed of approximately 130 m/s. TEC values at low and mid-latitudes nearly doubled during the main phase of the magnetic storm, with disturbances lasting 5–7 hours. In the EIA region, the height of the *F*2 layer increased significantly, attributed to an increase in eastward electric field strength. The dynamics of nighttime TEC values remain poorly understood.

The authors investigated mid-latitude blob-like structures along equatorial plasma bubbles over the East Asian region. These structures moved westward over thousands of kilometers and extended up to 40°N in latitude. The TEC enhancements within these structures were approximately 50 TECU (Sun et al.,2024a). Using multi-instrumental observations of the storm effects, the authors studied the complex of ionospheric fluctuations at low and mid-latitudes (Sun et al.,2024b). The amplitude of total electron content (TEC) oscillations reached up to 10 TECU. These disturbances originated at high latitudes and propagated equatorward as large-scale traveling ionospheric disturbances (TIDs). The most pronounced and complex fluctuations were observed at low latitudes, shaped by dynamic processes operating in both equatorial and high-latitude regions.

Thus, a series of studies has focused on global ionospheric disturbances caused by the storm of May 10–12, 2024. These disturbances are best described for the American region and the EIA area. An urgent task is to conduct a more detailed examination of the features of magnetic and ionospheric storms for the Chinese region.

This study presents the results of analyzing temporal variations in the geomagnetic field level, TEC, and parameters from a network of ionosondes for the Chinese region.

The paper is organized as follows. After analyzing the state of space weather, it briefly describes the instruments and methods used. This is followed by an analysis of the results of geomagnetic field variation observations at nine magnetic stations, variations in vertical sounding ionogram parameters, and TEC. The discussion is then followed by a summary of the main results.

2 Data and Methodology

To describe the state of space weather, this study is begun with the analysis of variations in the main solar wind parameters (**Figure 1**).

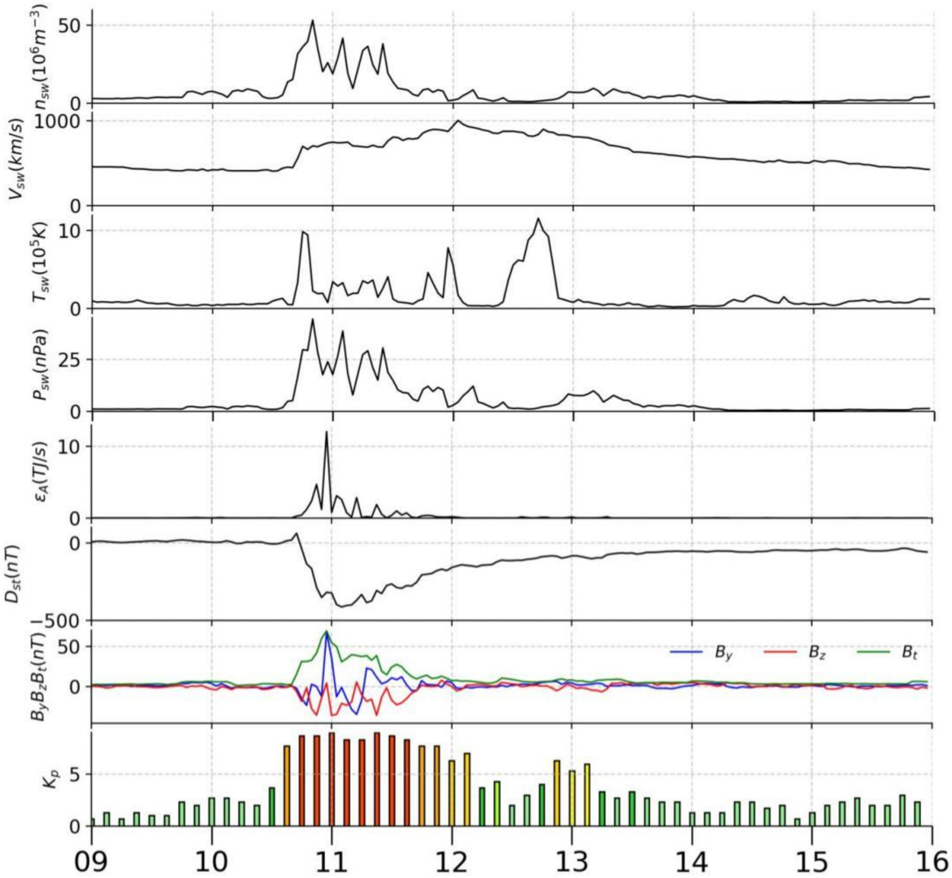

Figure 1. Temporal variations of space weather parameters from May 9 to May 15, 2024. Measured density, n_{sw}, temperature T_{sw}, radial velocity, V_{sw}, of solar wind, calculated dynamic pressure p_{sw}, measured B_z and B_y components and the total value of the interplanetary magnetic field; calculated energy, ε_A, transferred from the solar wind into the Earth's magnetosphere per until time; K_p- and D_{st}-index. (Retrieved from https://omniweb.gsfc.nasa.gov/form/dx1.html.)

On May 10 and 11, 2024, several particle density spikes in the solar wind from 2×10^6 m^{-3} to ~$(3.5–5)\times10^7$ m^{-3} were observed. The solar wind particle speed increased from about 400 km/s to 750–1000 km/s after 16:00 (hereinafter Universal Time) on May 10, 2024, and this increased speed persisted for at least six days. From 16:00 on May 10, 2024, to 21:00 on May 12, 2024, numerous spikes in the temperature of solar wind particles were recorded, from ~10^5 K to $(4–12)\times10^5$ K. From 16:00 on May 10, 2024, to the end of May 13, 2024, multiple dynamic pressure spikes were noted, ranging from ~1 nPa to ~5–45 nPa.

Next, the variations in the B_y and B_z components of the interplanetary magnetic field were described, as well as its total value. On May 10 and 11, 2024, the B_y component fluctuated between –34 nT and 68 nT, while the B_z component varied from –35 nT to 8 nT. The negative values of the B_z component indicated the onset of a geomagnetic storm. The B_t values changed within the range from 0 nT to 70 nT.

The Akasofu's epsilon parameter, which describes the power of magnetic field entering the magnetosphere, increased on May 10–11, 2024, from ~1 GJ/s to 15 TJ/s.

The planetary K_p index, which characterizes the intensity of geomagnetic storms, increased on May 10–11, 2024, from ~1 to 6–9. At $K_p = 9$, a magnetic storm of G5 type (extreme storm) occurred.

Approximately from 18:00 on May 10, 2024, to 04:00 on May 11, 2024, the main phase of the geomagnetic storm took place, with $D_{st\min} \approx -412$ nT. The recovery phase of this storm lasted for at least six days.

To investigate the manifestations of the geospace storm during May 10–12, 2024, in the magnetic field and ionosphere, measurements from a network of magnetometers, ionosondes, and Global Navigation Satellite System (GNSS) receivers were utilized. The spatial distribution of the observational instruments deployed over the Chinese region is presented in **Figure 2**. As shown in **Figure 2**, the measurement network covered an area spanning approximately 3300 km in both latitude and longitude.

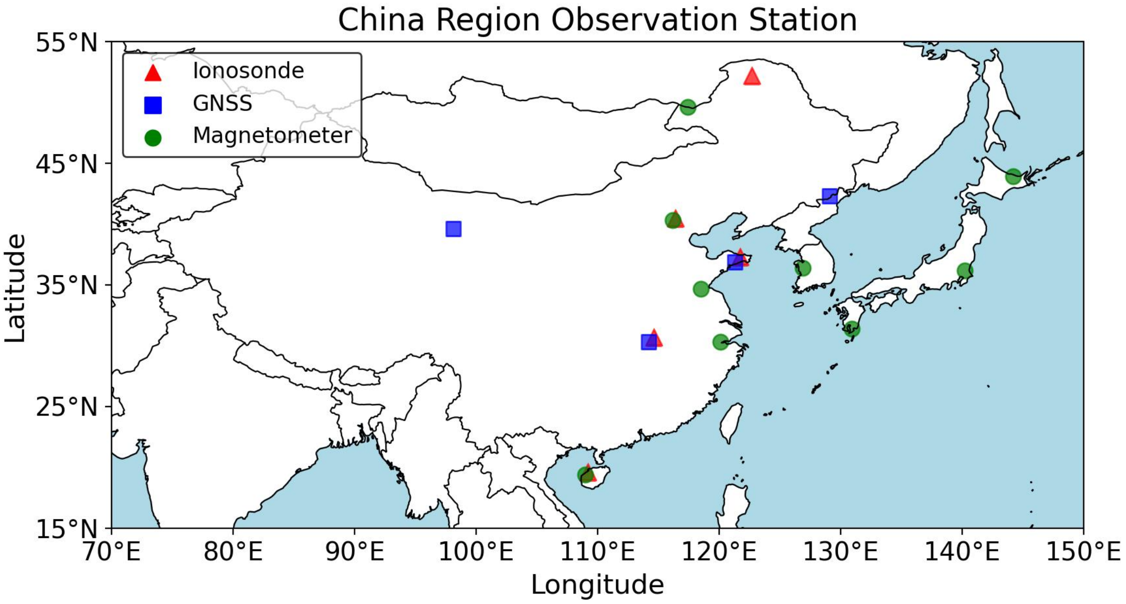

Figure 2. Location of stations for observing May 10–12, 2024, storm (Green circles is magnetometers, red triangles is ionosondes, blue squares is satellite stations).

2.1. Magnetometer Network

A list of the nine magnetometers belonging to the Intermagnet network (https://intermagnet.org) is provided in **Table 1**. The temporal resolution of the magnetometric measurements is 1 min, and the amplitude resolution is 1 nT.

Table 1. General information about magnetometric network.

Station	Latitude(MLAT)	Longitude(MLON)	Instrument	Sampling Interval
Hainan	19.4°N(8.7°N)	109°E(117.6°E)	Fluxgate Magnetometer	1s
Hangzhou	30.3°N(20.2°N)	120.1°E(187.6°E)	Fluxgate Magnetometer	1s
Kanoya	31.4°N(22.3°N)	130.9°E(197.4°E)	Fluxgate Magnetometer	1s
Linyi	34.7°N(25.8°N)	118.5°E(185.2°E)	Fluxgate Magnetometer	1s
Kakioka	36.2°N(28°N)	140.2°E(206.2°E)	Fluxgate Magnetometer	1s
Cheongyang	36.4°N(27.1°N)	126.9°E(194.5°E)	Fluxgate Magnetometer	1s
Beijing	40.3°N(31.7°N)	116.2°E(181.6°E)	Fluxgate Magnetometer	1min
Memambetsu	43.9°N(37°N)	144.2°E(210.2°E)	Fluxgate Magnetometer	1s
Manzhouli	49.6°N(42.5°N)	117.4°E(183°E)	Fluxgate Magnetometer	1s

The peak-to-peak amplitudes of variations in the *X*-, *Y*-, and *Z*-components of the geomagnetic field were subject to analysis. Therefore, the constant component was first removed from the original signal.

For a more detailed analysis of the recurring spikes in the component levels, a systems spectral analysis was applied, as described in (Chernogor,2008).

2.2. Ionosonde Network

Detailed information on the ionosonde stations is provided in **Table 2**. As indicated in **Table 2**, the ionosondes are distributed across both low- and mid-latitude regions. Notably, the Hainan and Wuhan stations are situated within the Equatorial Ionization Anomaly (EIA) zone. The northernmost station, Mohe, is located at a latitude of 52°N. The ionosonde measurements had a temporal resolution of 15 minutes and a frequency resolution of approximately 0.1 MHz.

Table 2. General information about ionosonde network.

Station	Latitude(MLAT)	Longitude(MLON)	Instrument	Sampling Interval
Hainan	19.4°N(8.7°N)	109°E(117.6°E)	DPS-4D	15min
Wuhan	30.5°N(20.5°N)	114.4°E(183.5°E)	DPS-4D	15min

Weihai	37.1°N(28.6°N)	121.5°E(189.2°E)	DPS-4D	15min
Beijing	40.3°N(31.7°N)	116.2°E(181.6°E)	DPS-4D	15min
Mohe	52°N(45.5°N)	122.5°E(186.5°E)	DPS-4D	15min

2.3. Satellite Stations

A list of GNSS stations is provided in **Table 3** (www.meridianproject.ac.cn). **Table 3** summarizes the GNSS stations used in this study, all of which are located at mid-latitudes within the Chinese region. For the analysis, data from satellites C1, C2, C3, C7, C9, C10, C16, C30, C36, C39, C40, and C46 were employed. The GNSS observations covered a spatial area of several thousand kilometers in both latitude and longitude.The error in estimating TEC is approximately 1 TECU (1 Total Electron Content Unit = 10^{16} electrons/m^{2}).

Table 3. General information about satellite stations.

Station	Latitude(MLAT)	Longitude(MLON)	Instrument	Sampling Interval
Wuhan	.30.5°N(20.5°N)	114.4°E(183.5°E)	GNSS Ionospheric TEC .Scintillation Monitor	1s
Weihai	37.1°N(28.6°N)	121.5°E(189.2°E)	GNSS Ionospheric TEC .Scintillation Monitor	1s
JiaYuguan	39.8°N(29.5°N)	98.3°E(166.8°E)	GNSS Ionospheric TEC .Scintillation Monitor	1s
Yanji	42.5°N(33.9°N)	129.3°E(197.8°E)	GNSS Ionospheric TEC .Scintillation Monitor	1s

3 Results of Observations

This section may be divided by subheadings. It should provide a concise and precise description of the experimental results, their interpretation, as well as the experimental conclusions that can be drawn.

3.1. Variations in the Geomagnetic Field Level

The temporal variations of the *X*- (north–south direction), *Y*- (west–east direction), and *Z*- (vertical direction) components of the geomagnetic field recorded at nine stations were subject to analysis (**Table 1**). The latitude of these stations ranged from 19.4°N to 49.5°N, covering low and mid-latitudes, including the EIA region. The longitude of the stations varied around 130°E.

The temporal variations of all three components of the geomagnetic field at the nine observation stations exhibited qualitatively similar patterns. As a representative example, a detailed description of the variations at the low-latitude Hainan station is provided in **Figure 3**. The corresponding temporal variations for the remaining eight stations are presented in the Supplement (Supplement **Figure S1–S8**).

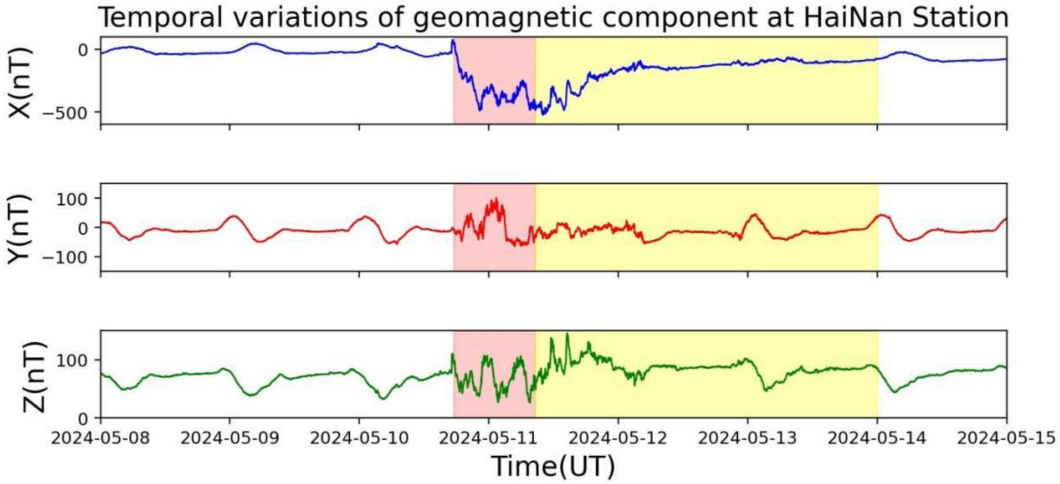

Figure 3. Temporal variations in the level of the X-, Y-, and Z-components of the geomagnetic field on May 8–14, 2024, at the Hainan station.The red-shaded region indicates the main phase of the geomagnetic storm, while the yellow-shaded region corresponds to the recovery phase.

Prior to the onset of the magnetic storm, the diurnal variations of the *X*-component did not exceed 67 nT. Around 18:00 UT on May 10, 2024, the *X*-component exhibited a sharp increase of approximately 100 nT over the course of about 1 hour, followed by a rapid decrease of approximately 600 nT. During this disturbance, six to seven prominent spikes were observed. The total duration of the disturbance was approximately 50 hours.

Before the storm, the diurnal variations in the Y-component did not exceed 86 nT. After 18:00 on May 10, 2024, the peak-to-peak amplitude of variations reached 166 nT, persisting for about 40–60 h. The number of spikes did not exceed four.

Prior to the magnetic storm, the diurnal variations in the *Z*-component reached up to 43 nT. Following the storm's onset, alternating-sign variations with a peak-to-peak amplitude of up to 119 nT and a duration of approximately 47 hours were recorded. A total of six to seven spikes were identified during this interval.

For all components, the largest variations in level occurred during the main phase and the beginning of the recovery phase, lasting about 15 h.

The main parameters of the disturbances in the *X*-, *Y*-, and *Z*-components of the magnetic field during the storm are presented in **Table 4**. From **Table 4**, it is evident that there was a tendency for the peak-to-peak amplitude of variations to increase with geographic latitude, except for the Hainan and Hangzhou stations, which are located within the EIA region. The *X*-component was most disturbed during the storm, while the *Z*-component was least disturbed. The duration of the disturbances was weakly dependent on latitude and was approximately 40–60 h.

Table 4. Main parameters of disturbances in the geomagnetic field component levels during the storm.

Station	Component	Maximum variation (nT)	Duration (h)	Period (min)
Hainan	*X*	598	68	200
	Y	166	54	90; 205
	Z	119	64	85; 195
Hangzhou	*X*	586	70	200
	Y	238	56	90; 200
	Z	100	58	200
Kanoya	*X*	550	60	200
	Y	260	44	90; 210
	Z	300	44	205
Kakioka	*X*	550	60	200
	Y	260	40	90; 205
	Z	108	44	200
Linyi	*X*	652	70	195
	Y	264	61	90; 220
	Z	120	64	200
Cheongyang	*X*	680	60	200
	Y	270	44	90; 205
	Z	150	50	200
Beijing	*X*	700	60	200
	Y	310	44	90; 205
	Z	140	56	205
Memambetsu	*X*	670	60	200
	Y	375	44	90; 200
	Z	220	40	205
Manzhouli	*X*	799	66	195
	Y	422	42	95; 205
	Z	412	45	205

3.2. Variations in Ionogram Parameters

The most important parameters of ionograms that describe the state of the ionosphere are the critical frequencies of the *E*, *F*1, and *F*2 layers, i.e., *fo*E, *fo*F1, and *fo*F2, their heights *h*m*E*, *h*m*F*1, and *h*m*F*2, and the minimum observed frequency of the reflected radio signal, $f_{\min}$. This frequency qualitatively characterizes the level of radio wave absorption in the lower ionosphere and thus the degree of disturbance in this part of the ionosphere. During the magnetic storm, the *E*-region was practically undisturbed, and the parameters *foE* and *h*m*E* are not considered in this paper.

The variations in ionogram parameters for the lowest-latitude station (Station Hainan) and the mid-latitude station (Station Mohe) will be considered in detail next.

3.2.1. Variations in *fo*F2

At the Hainan station, the *foF*2 values fluctuated significantly both before and after the storm (**Figure 4**). Prior to the storm, diurnal variations in *fo*F2 were weakly expressed, with maximum daytime values of *foF*2 ≈ 9 MHz and nighttime values dropping to approximately 4 MHz. After the onset of the storm, diurnal variations in *foF*2 became more pronounced. During midday, $foF2_{\max}$ remained about 9 MHz, while nighttime *foF*2 values decreased to 2 MHz. The duration of the ionospheric storm was approximately 50 h.

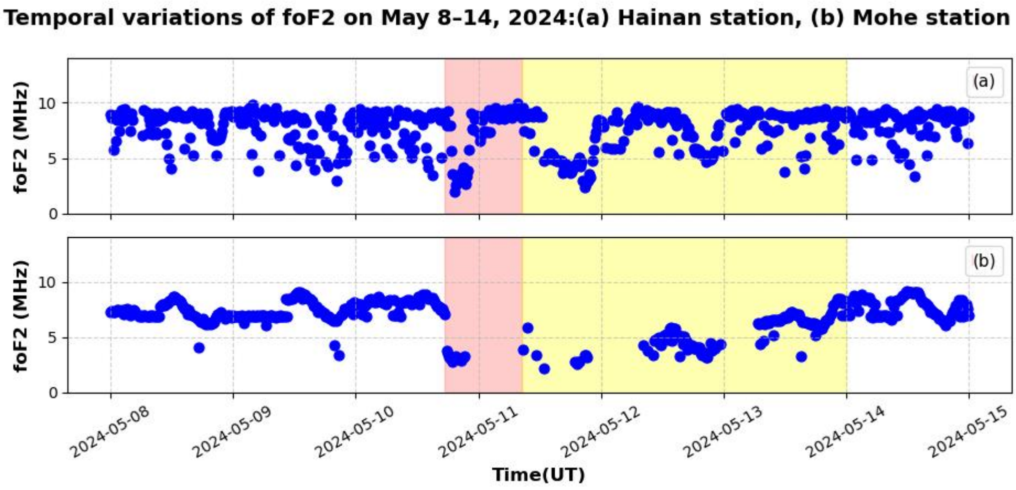

Figure 4. Temporal variations of foF2 on May 8–14, 2024: (a) Hainan station, (b) Mohe station.

At the Mohe station, the fluctuations were less pronounced compared to those at the Hainan station (**Figure 4**). Before the storm, maximum daytime values of *foF*2 ≈ 9 MHz, while nighttime values were approximately 6 MHz. After the storm began, daytime *foF*2 ≈ 2 MHz, and nighttime *foF*2 ≈ 3 MHz. The ionospheric storm lasted approximately 50 h. On May 13, 2024, a negative ionospheric storm persisted, transitioning into a positive ionospheric storm at the beginning of May 14. In this case, *fo*F2 increased from 7 MHz to 9 MHz.

At the Wuhan station, pre-storm daytime *fo*F2 values reached 12 MHz, while nighttime values dropped to ~7 MHz (Supplement **Figure S9**). After the storm began, daytime *fo*F2 ≈ 4–8 MHz, and nighttime *fo*F2 ≈ 4 MHz. The duration of the ionospheric storm was approximately 54 h.

At the Weihai station, pre-storm *fo*F2 values did not exceed 10–11 MHz during the day and decreased to ~3 MHz at night (Supplement **Figure S9**). At the end of May 10 and throughout May 11–12, 2024, daytime *fo*F2 values dropped to 4–6 MHz, while nighttime values decreased to 3 MHz. The duration of the ionospheric storm did not exceed 50 h.

3.2.2. Variations in *h*m*F*2

Before the storm, the *h*m*F*2 values at the Hainan station rarely exceeded 400 km during the daytime and dropped to 200 km at night (**Figure 5**). On May 10, 2024, around midday, *h*m*F*2 reached 500–700 km. From 18:00 on May 10, 2024, to 12:00 on May 12, 2024, *h*m*F*2 values fluctuated significantly between ~100 km and ~700 km. After the storm began on May 10, 2024, nighttime *h*m*F*2 values increased to 500–530 km and then gradually decreased to ~100 km. On May 11 and 12, 2024, daytime *h*m*F*2 values reached 600–700 km, while nighttime values decreased to 100–200 km. The duration of the ionospheric storm was approximately 50 h.

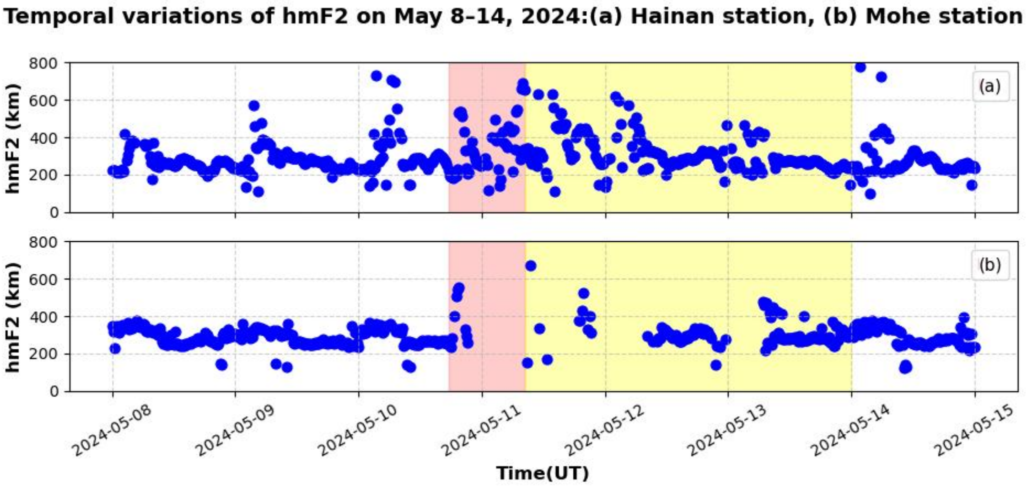

Figure 5. Temporal variations of hmF2 on May 8–14, 2024: (a) Hainan station, (b) Mohe station.

At the Mohe station, *h*m*F*2 values reached ~370 km before the storm during the daytime and dropped to ~250 km at night (**Figure 5**). After the storm began around 18:00 on May 10, 2024, *h*m*F*2 fluctuations increased sharply, ranging from 150 km to 500–680 km. The duration of the storm was approximately 40 h.

Before the storm, *h*m*F*2 at the Wuhan station fluctuated within 200–300 km, with occasional increases from ~100 km to 500 km (Supplement **Figure S10**). Almost immediately after the storm began, *h*m*F*2 values increased to ~500 km. For over 54 h, *h*m*F*2 fluctuated between ~100–120 km and 600–700 km. The diurnal behavior of *h*m*F*2(*t*) was significantly disrupted.

At the Weihai station, pre-storm *h*m*F*2 values were approximately 200–300 km. Nighttime values of this height were practically not recorded (Supplement **Figure S10**). After the storm began, *h*m*F*2 values fluctuated within 200–400 km. The duration of ionospheric disturbances was about 50 h.

3.2.3. Variations in *foF*1

The *F*1 layer was not consistently observed. At the Hainan station, prior to the storm, the *foF*1 frequency fluctuated within the range of 6–8 MHz (**Figure 6**). After the storm began, the fluctuation range expanded to 4–8 MHz. The duration of disturbances was approximately 50 h.

At the Mohe station, the *F*1 layer was rarely recorded. Occasionally, *foF*1 ≈ 2–6 MHz (**Figure 6**). The storm had little impact on the *F*1 layer at these latitudes.

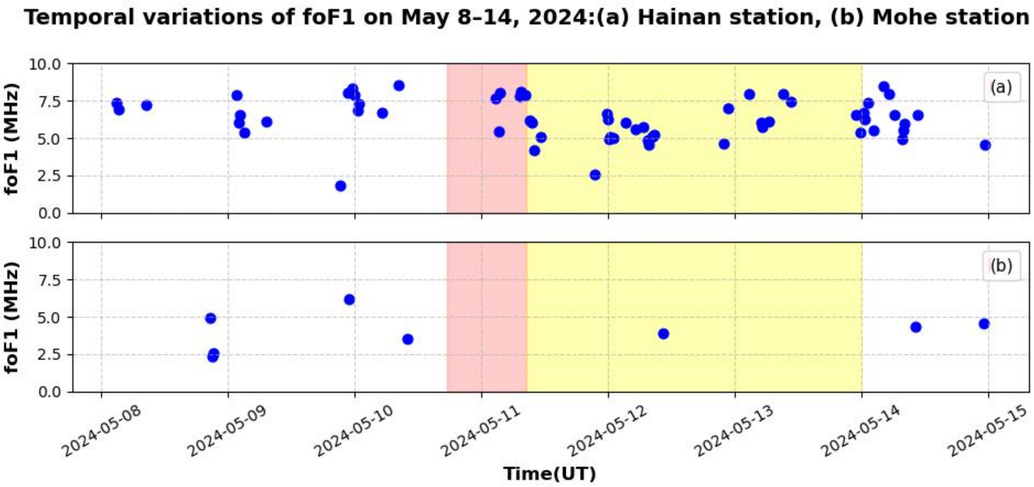

Figure 6. Temporal variations of foF1 on May 8–14, 2024: (a) Hainan station, (b) Mohe station.

https://doi.org/10.5194/egusphere-2025-3661
Preprint. Discussion started: 14 August 2025

At the Wuhan station, the *F*1 layer was frequently observed (Supplement **Figure S11**). From May 8 to May 12, 2024, *fo**F*1 ≈ 2–6 MHz. The storm had almost no effect on *fo**F*1 values.

At the Weihai station, prior to the storm, *fo**F*1 ≈ 5–6 MHz, while after the storm *fo**F*1 ≈ 2–6 MHz, indicating a noticeable decrease in frequency (Supplement **Figure S11**).

3.2.4. Variations in *h*m*F*1

On May 8 and 9, 2024, at the Hainan station, *h*m*F*1 values predominantly fluctuated between 200 km and 400 km (**Figure 7**). On May 10, 2024, prior to the storm, *h*m*F*1 values occasionally increased from 200 km to 500–700 km. After the storm began, the fluctuation range increased from ~100 km to 700–740 km. The duration of disturbances in *h*m*F*1 values was approximately 50 h.

At the Mohe station, prior to the storm, *h*m*F*1 ≈ 250–370 km (**Figure 7**). After 18:00 on May 10, 2024, the fluctuation range increased from ~150 km to 550 km and then up to 680 km. The duration of disturbances in this height did not exceed 40 h.

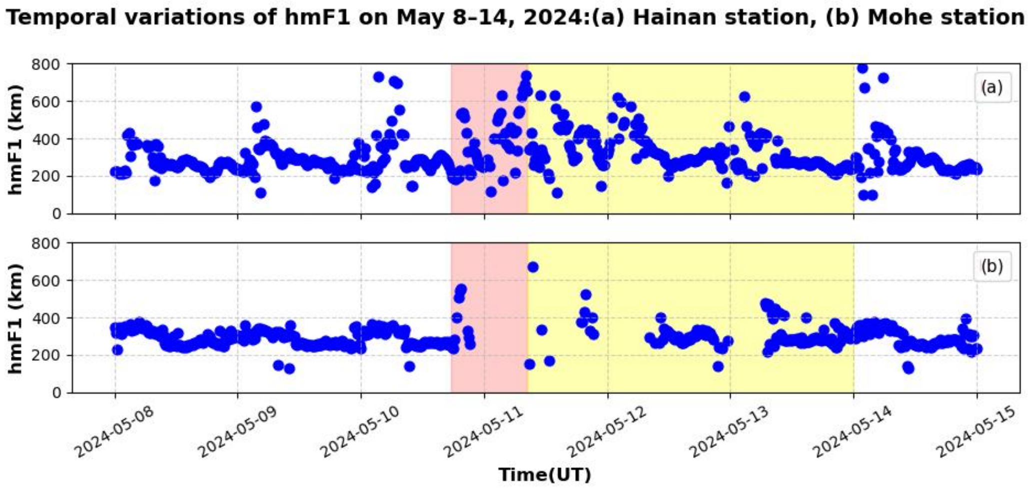

Figure 7. Temporal variations of hmF1 on May 8–14, 2024: (a) Hainan station, (b) Mohe station.

Fluctuations at the Wuhan station prior to the storm were relatively small (200–300 km) (Supplement **Figure S12**). Occasionally, *h*m*F*1 values decreased to ~100–120 km and increased to ~400–500 km. After the storm began, the variation range of *h*m*F*1 increased from ~100–120 km to ~700 km. This lasted for more than 55 h.

At the Weihai station, prior to the storm, *h*m*F*1 varied within ~200–380 km (Supplement **Figure S12**). After the storm began, for approximately 50 h, *h*m*F*1 values fluctuated from ~200 km to ~400–450 km.

https://doi.org/10.5194/egusphere-2025-3661
Preprint. Discussion started: 14 August 2025

3.2.5. Variations in $f_{\min}$

On May 8–9, 2024, at the Hainan station, the values of $f_{\min}$ fluctuated within the range of ~1–5 MHz (**Figure 8**). The lowest values were observed during nighttime, while the highest values occurred during daytime, with $f_{\min} \approx 3$–4 MHz. On May 10, 2024, daytime $f_{\min}$ did not exceed 3–3.5 MHz, and nighttime $f_{\min} \approx 1$–1.9 MHz. Similarly, on May 11, 2024, daytime $f_{\min} \approx 3$–3.5 MHz, while nighttime values remained around 1–1.9 MHz. On May 12, 2024, daytime $f_{\min}$ exhibited a wider spread from 1.8 MHz to 4.4 MHz but predominantly stayed near 3 MHz. On May 13 and 14, 2024, temporal variations in $f_{\min}(t)$ corresponded to an undisturbed ionosphere.

At the Mohe station from May 8 to 14, 2024, the range of $f_{\min}$ was relatively narrow: during daytime $f_{\min} \approx 3$–3.8 MHz, and during nighttime $f_{\min} \approx 1.6$–2 MHz (**Figure 8**). On May 11, 2024, $f_{\min}$ values were episodically absent early in the day and around midday. Starting from the second half of May 12, 2024, ionospheric disturbances lasting approximately 40 h were no longer observed.

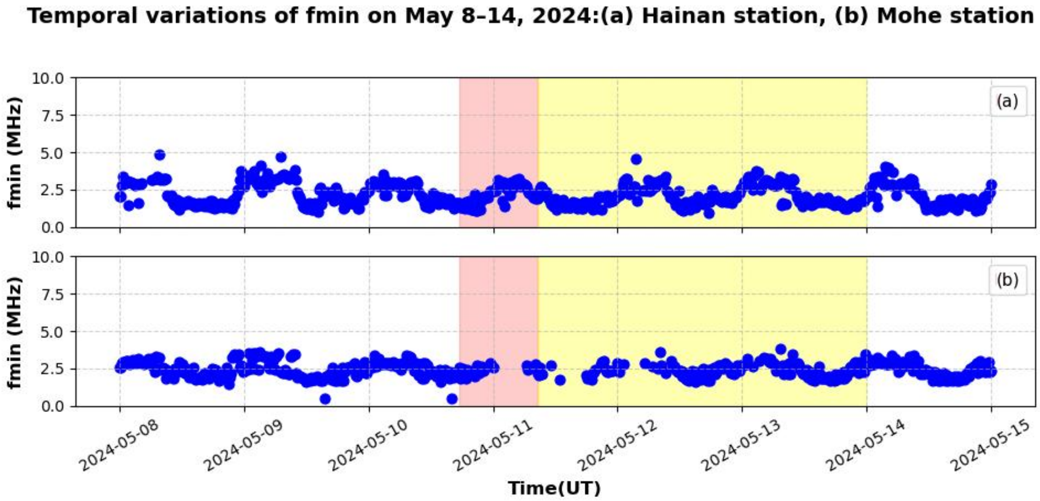

Figure 8. Temporal variations of $f_{\min}$ on May 8–14, 2024: (a) Hainan station, (b) Mohe station.

Prior to the storm at the Wuhan station, $f_{\min}$ varied from ~1.5 MHz at night to 3–3.2 MHz during daytime (Supplement **Figure S13**). Early on May 11, 2024, $f_{\min}$, while fluctuating, increased from 3 MHz to 4.2–4.6 MHz. During nighttime on May 11, $f_{\min}$ remained undisturbed (1.5–1.9 MHz). Almost identical picture was observed on May 12, 2024. From May 13 onward, $f_{\min}$ returned to undisturbed values.

At the Weihai station before the storm, daytime $f_{\min} \approx 3$ MHz and nighttime $f_{\min} \approx 1.8$–1.9 MHz (Supplement **Figure S13**). After the onset of the storm, the range of $f_{\min}$ expanded slightly (from 1 MHz to 3.8 MHz), lasting for about 60 h.

Overall, the storm had a minor impact on $f_{\min}$ values, indicating that the lower ionosphere at low and mid-latitudes remained largely undisturbed in the course of the storm.

3.3. Variations in TEC

Before the onset of the storm, the TEC values at the Wuhan station during daytime reached 60–70 TECU, while nighttime values decreased to ~20 TECU (**Figure 9**). On May 11, 2024, daytime TEC values decreased by 30–40 TECU (~43–50%), whereas nighttime TEC values increased to 55 TECU (by 175%). On May 12, 2024, TEC values decreased to 20–30 TECU (by ~60–70%).

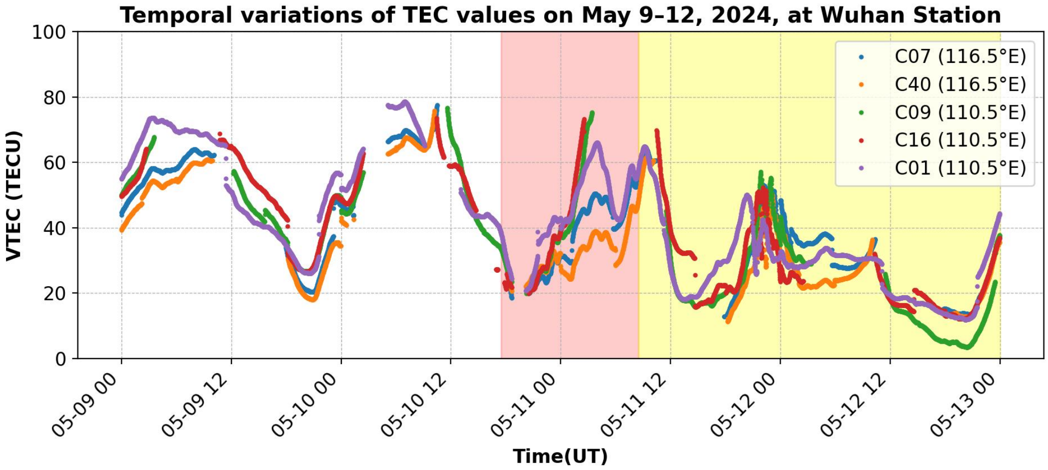

Figure 9. Temporal variations of TEC values on May 9–12, 2024, at the Wuhan station.

At the Weihai station on May 9 and 10, 2024, daytime TEC values were approximately 50–55 TECU, while nighttime values were close to 20–25 TECU (**Figure 10**). On May 11, 2024, TEC values in the first half of the day dropped to ~20–30 TECU (by ~55–60%), and in the second half of the day they decreased by 10–20 TECU (~20–36%). Conversely, nighttime TEC values increased from ~20 TECU to ~40 TECU (by 100%). On May 12, 2024, daytime TEC values dropped to 20 TECU (decrease by ~55–60%).

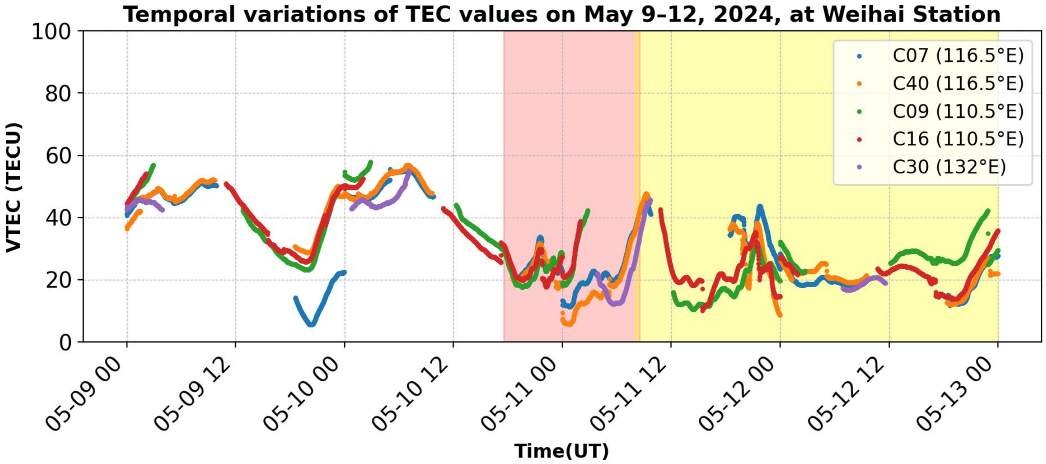

Figure 10. Temporal variations of TEC values on May 9–12, 2024, at the Weihai station.

Prior to the storm, at the Jiayuguan station, daytime TEC values reached 60–70 TECU, while nighttime values decreased to 20–30 TECU (**Figure 11**). On May 11, 2024, daytime TEC values dropped by 30–40 TECU (~50–57%), and nighttime values decreased by 10–15 TECU (~50%). On May 12, 2024, daytime reductions in TEC did not exceed 20–30 TECU (~30–40%), while nighttime reductions were approximately 10 TECU (~30–50%).

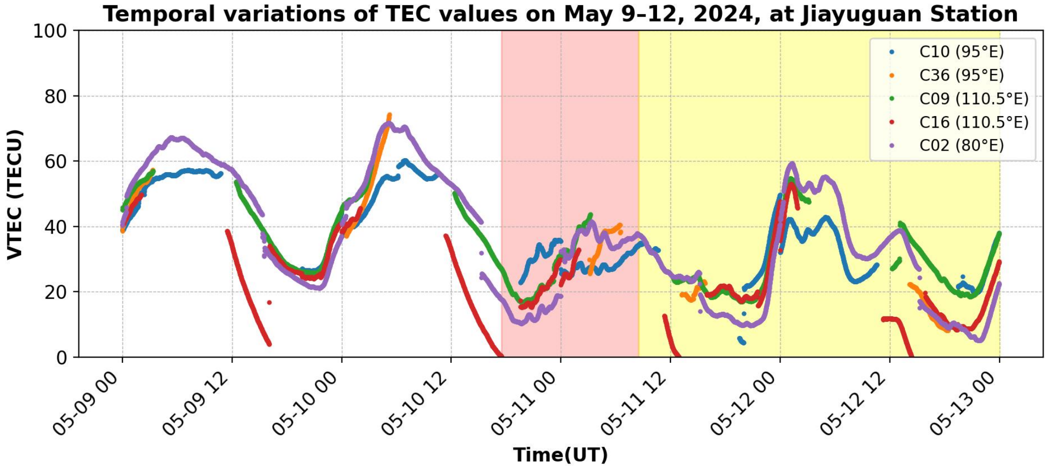

Figure 11. Temporal variations of TEC values on May 9–12, 2024, at the Jiayuguan station.

At the Yanji station before the storm, daytime TEC values reached 45–50 TECU, while nighttime values dropped to 20–25 TECU (**Figure 12**). On May 11, 2024, daytime TEC values decreased to 20–30 TECU (by ~40–60%), while nighttime values increased to 40–50 TECU (1.7–2 times). On May 12, 2024, daytime values decreased to 20 TECU (40%), and nighttime values dropped to ~10 TECU (30%).

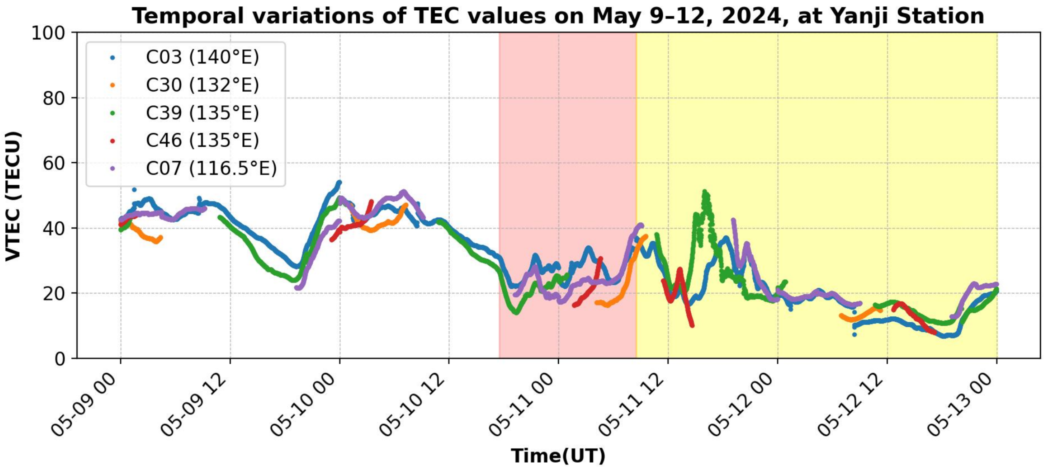

Figure 12. Temporal variations of TEC values on May 9–12, 2024, at the Yanji station.

3.4. Results of Systems Spectral Analysis

Figure 3 and Supplement **Figure S1–S8** illustrate that all components of the geomagnetic field exhibited quasi-periodic variations over time. To investigate these temporal behaviors in greater detail, spectral analysis techniques were employed. Specifically, the systems spectral analysis (SSA) (Chernogor,2008) was utilized, incorporating three mutually complementary integral transforms. The first is the Short-Time Fourier Transform (STFT), which provides optimal time resolution for analyzing rapidly evolving signals. The second is the Adaptive Fourier Transform (AFT), which adapts to the local oscillation period, thereby offering enhanced resolution in the frequency domain. The third is the Wavelet Transform (WT) based on the Morlet wavelet, often referred to as a "mathematical microscope" due to its capability to resolve oscillations across a wide range of amplitudes and timescales.

Example of SSA results for the Hainan station are shown in **Figure 13–15**, with additional data for two other stations provided in the Supplement (Supplement **Figure S14–S19**). **Figure 13** shows the dominant oscillation with a period of $T \approx$ 200 min. For the Y-component, the most significant oscillations exhibit periods of 200 min and 85 min (**Figure 14**), while for the Z-component, oscillations with periods of 195 min and 85 min predominate (**Figure 15**).

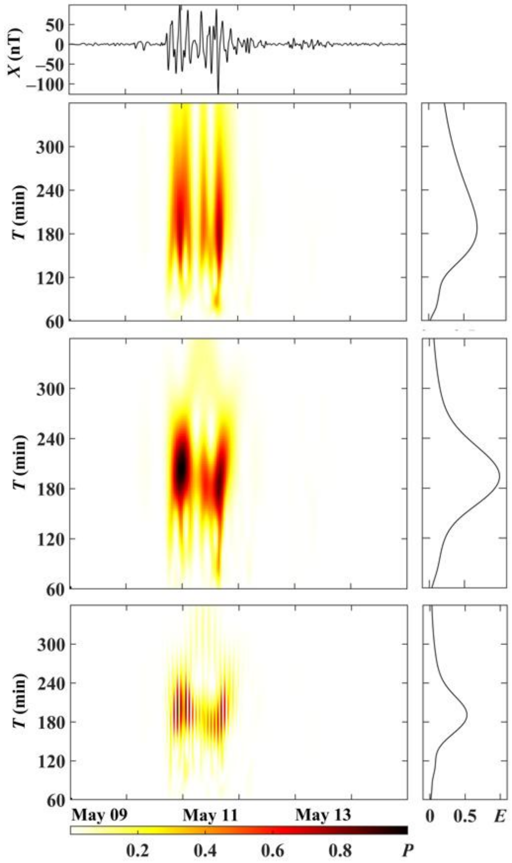

Figure 13. SSA results for variations of the Hainan station X-component fluctuation levels on 9−14 May 2024. Panels from top to bottom: the detrended signal, the results of the short-time Fourier transform, the adaptive Fourier transform, and the Morlet wavelet transform. The right small window illustrates the distribution of relative energy of oscillations across different periods.

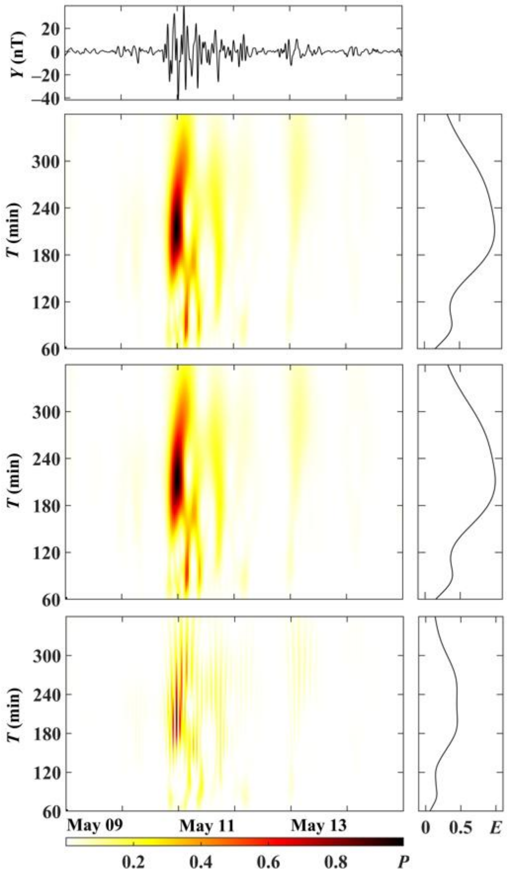

Figure 14. The same as in Figure 13 but for the Y-component.

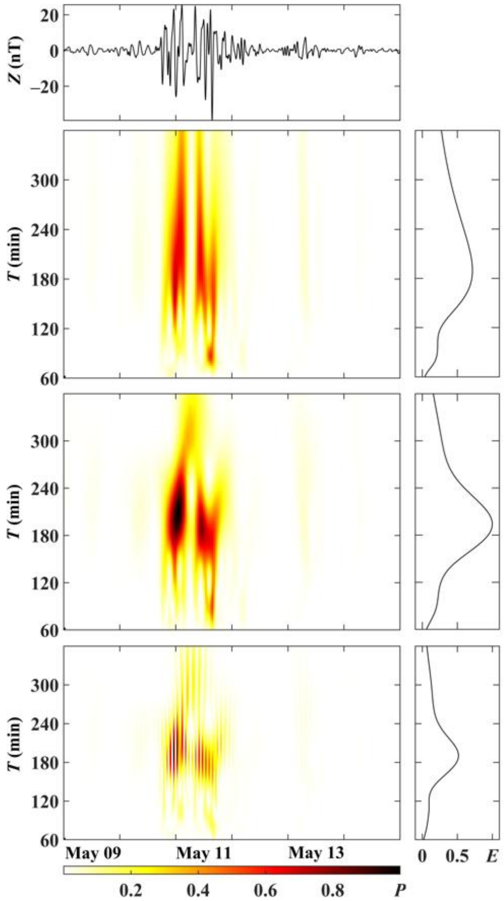

Figure 15. The same as in Figure 13 but for the Z-component.

A summary of predominant oscillation periods is presented in **Table 4**. The data indicate that the primary period for all geomagnetic field components at all stations is approximately 200 min. For the *Y*-component, an oscillation with a period of about 90 min is also observed, though its amplitude is several times smaller than that of the $T \approx 200$ min oscillation.

4 Discussion

405 The variations in geomagnetic field intensity, ionogram parameters, and total electron content (TEC) associated with the geospace storm over China during May 10–12, 2024, are discussed separately.

4.1. Geomagnetic Field Variations

The described geomagnetic storm is among the strongest in the 25th solar activity cycle. Such intense storms have not occurred for approximately 20 years, dating back to 2003. The Akasofu's epsilon parameter, which describes the power of the solar wind magnetic pressure on the magnetosphere, reached 15 TW/s, corresponding to a super extreme storm type, with a magnetospheric storm index MSI6 and $G_{st} \approx 42$ dB (Chernogor,2025).

The energy of the magnetic storm, determined by the corrected D_{st} index, reached 20 PJ, corresponding to a G5 storm type (extreme storm) with $K_p = 9$ (Chernogor,2025).The energy and power of the geospace storm, determined by the solar wind dynamic pressure, were close to 6.5 EJ and 0.4 PW, respectively, categorizing it as a severe storm (Chernogor,2025).

The maximum peak-to-peak amplitude of variations in the *X*-component for stations in the Chinese region was 550–800 nT. For the *Y*- and *Z*-components, they were within 166–422 nT and 100–412 nT, respectively. Generally, with increasing latitude, a tendency toward an increase in the peak-to-peak amplitude of variations of all components was observed. However, this tendency was somewhat disrupted for stations located within the EIA region. The significant decrease in the *X*-component level is attributed to the penetration of the electric field from the magnetosphere into the ionosphere, where electric currents flow, forming the *X*-component level.

Our results are in good agreement with the findings in (Zhang R.et al.,2024). The SSA revealed that the spectrum of geomagnetic field variations was dominated by oscillations with periods of 200 min and 90 min. These observed quasi-periods are due to recurring spikes in solar wind parameters.

4.2. Variations in Ionogram Parameters

During geospace storms, the *F*2 layer of the ionosphere is the most significantly disturbed, as evidenced by variations in *fo**F*2 and *h*m*F*2 (Shi et al.,2023,2025). The ionospheric storm parameters were strongly dependent on the latitude of the observation station. In the Chinese region, latitude ranged approximately from 30.5°N to 52°N.

At the low-latitude station Hainan, on May 11, 2024, the ionospheric storm was almost undetectable in *fo**F*2 values during daytime (**Table 5**). At the same time, the peak-to-peak fluctuations of *h*m*F*2 increased to 600 km, compared to less than 200 km on the reference day of May 8, 2024. At this station during nighttime on May 10, 11, and 12, 2024, *fo**F*2 values decreased to approximately 2 MHz, 2 MHz, and 3 MHz, respectively, whereas they were 4–6 MHz on the reference day. The features of variations in *fo**F*2 at the Hainan station are attributed to the influence of the EIA.

Table 5. Main parameters of the ionospheric storm based on the ionosonde data.

Station	Time	$foF2_0$ (MHz)	$foF2$ (MHz)	I_{NIS} (dB)	Storm level
Hainan	Day	9	9	0	–

	Night	4	2	6	Severe
Wuhan	Day	12	6	6	Severe
	Night	7	3.5	6	Severe
Weihai	Day	10–11	4–6	5.2–8	Severe
	Night	3	3	0	–
Mohe	Day	9	3	9.5	Extreme
	Night	3	3	6	Severe

At other stations, ionospheric storm effects were more pronounced. At the Wuhan station, both daytime and nighttime *f*o*F*2 values decreased by half on average (**Table 5**). While *h*m*F*2 values on May 8, 2024 (reference day), varied approximately from 200 km to 300 km, they fluctuated within a range of ~200–700 km on May 11 and 12, 2024.

At the Weihai station, significant variations in *f*o*F*2 were observed during daytime. The *f*o*F*2 values decreased to 4–6 MHz compared to the reference day values of 10–11 MHz (**Table 5**). Nighttime *f*o*F*2 values were almost not disturbed. Variations in *h*m*F*2 were also relatively minor.

The largest daytime variations in *f*o*F*2 were recorded at the Mohe station. On the reference day, *f*o*F*2 ≈ 9 MHz, whereas on May 11, 2024, *f*o*F*2 ≈ 2–4 MHz, and on May 12, 2024, *f*o*F*2 ≈ 6 MHz (**Table 5**). On the reference day *h*m*F*2 ≈ 250–350 km, and on May 10–11, 2024, *h*m*F*2 ≈ 200–550 km.

A significant decrease in *f*o*F*2 and an increase in *h*m*F*2 indicate that a negative ionospheric storm occurred in the Chinese region. The intensity and type of the storm can be effectively evaluated using the negative ionospheric storm index (NISI) (Chernogor,2025):

$$I_{NIS} = 20\log\frac{foF2_0}{foF2_{\min}}, \text{ dB} \qquad (1)$$

where $foF2_0$ is the frequency value on the reference day, and $foF2_{\min}$ is the frequency value at the same time on the storm day. The results of the I_{NIS} calculations are presented in **Table 5**. From **Table 5**, it can be seen that I_{NIS} values range approximately from 6 dB to 8 dB, corresponding to a severe storm (Chernogor,2025). Only for the northernmost station Mohe during daytime did $foF2_0/foF2_{\min} \approx 3$, resulting in $I_{NIS} \approx 9$ dB, which corresponds to an extreme storm (Chernogor,2025).

According to the seven-level scale, severe and extreme storms correspond to NISI4 and NISI5 storm types (Chernogor,2025).

The described features of the ionospheric storm on May 10–12, 2024, are consistent with the findings in (Zhang R.et al.,2024) and significantly complement them.

https://doi.org/10.5194/egusphere-2025-3661
Preprint. Discussion started: 14 August 2025

4.3. Variations in TEC

On all stations, daytime TEC values on the reference day were $N_{V0} \approx$ 50–70 TECU, while on May 11–12, 2024, N_V did not exceed 20–30 TECU (**Table 6**). At nighttime, $N_{V0} \approx$ 20 TECU, and $N_V \approx$ 10 TECU. This indicates that during the negative ionospheric storm, TEC values decreased by a factor of 2–3. At the same time, electron density N decreased by a factor of 4–9, since $N_0/N_{\min} = (foF2_0/foF2_{\min})^2 \approx 4–9$. The index values

$$I_{VNIS} = 10\log\frac{N_{V0}}{N_{V\min}}, \text{dB} \qquad (2)$$

for this storm ranged between 3–4 dB, corresponding to a severe storm. Only at the Wuhan station during daytime did the I_{VNIS} values reach 4.8 dB, characteristic of an extreme storm. A comparison of I_{NIS} and I_{VNIS} shows that I_{NIS} is always greater than I_{VNIS}. This difference arises because I_{NIS} quantifies variations in N specifically at the $F2$ layer peak, which experiences the most significant disturbances during the ionospheric storm. In contrast, I_{VNIS} describes the decrease in TEC not only at $hmF2$, but also the decrease in N both below $hmF2$ and above $hmF2$. Since N remains nearly unchanged at heights $h < 200$ km and $h > 600$ km, then $I_{NIS} > I_{VNIS}$.

Table 6. Main parameters of the ionospheric storm based on the TEC data.

Station	Time	N_{V0} (TECU)	N_V (TECU)	I_{VNIS} (dB)	Storm level
Wuhan	Day	60–70	20–30	4.8–3.7	Extreme
	Night	20	10	3	Severe
Weihai	Day	50	20	4	Severe
	Night	20	10	3	Severe
Jiayuguan	Day	60–70	30	3–3.7	Severe
	Night	20	10	3	Severe
Yanji	Day	50	20	4	Severe
	Night	20	10	3	Severe

There were several reasons for the negative ionospheric storm. First, the penetration of the magnetospheric electric field into the ionosphere. Second, an enhancement of the westward electric field at ionospheric heights. Due to the increase in convection speed, thermospheric chemical composition was disrupted, the O/N_2 ratio decreased. The equatorward thermospheric winds, and consequently the associated plasma transport, played a critical role in the storm dynamics. These processes collectively contributed to the development of a severe ionospheric storm.

5 Summary

In this paper, multi-instrument observational techniques and systems spectral analysis were utilized to investigate magnetic-ionospheric disturbances during the geospace storm of May 10–12, 2024. The main findings of the research on these disturbances in the Chinese region are summarized as follows.

The geospace storm, classified as a severe storm, triggered severe magnetic and ionospheric storms. During certain time intervals, the ionospheric storm transitioned from a severe storm to an extreme storm. The X-component's maximum peak-to-peak amplitude of variations reached 550–800 nT and the *Z*-component was the least disturbed (100–412 nT), while the *Y*-component exhibited a peak-to-peak amplitude of variations between 166 and 422 nT during the magnetic storm. The duration of geomagnetic field disturbances was approximately 40–60 h. A tendency for the peak-to-peak amplitude of variations to increase with geographic latitude was observed. The spectrum of geomagnetic field variations was dominated by oscillations with periods of 200 min and 90 min. Furthermore, during the negative ionospheric storm, *f*o*F*2 values decreased by a factor of 2–3, while electron density decreased by a factor of 4–9. At the same time, *h*m*F*2 values increased by 200–300 km. Based on TEC measurements, during the negative ionospheric storm, TEC values decreased by a factor of 2–3, corresponding to reductions of 30–40 TECU during the day and 10 TECU at night. The ionospheric storm over the Chinese region was classified as a severe storm, lasting approximately 50 h.

The above analysis elucidates the following physical mechanisms. The negative ionospheric storm was primarily driven by the penetration of magnetospheric electric fields into the ionosphere, the enhancement of plasma convection, disturbances in the thermospheric chemical composition, the intensification of thermospheric winds, and plasma transport processes occurring in both vertical and horizontal directions. The combined effects of these factors led to significant plasma depletion in the ionosphere during the storm period.

Author Contributions

For research articles with several authors, a short paragraph specifying their individual contributions must be provided. The following statements should be used "Conceptualization, L.Ch. ; methodology, L.Ch. ; software, X.T. and M.Sh; validation, X.T., L.Ch., Y.L., Zh.J., M.Sh., Ye.Zh., Y.Zh. ; formal analysis, X.T., L.Ch., Y.L., Zh.J., M.Sh., Ye.Zh., Y.Zh. ; investigation, X.T., L.Ch., Y.L., Zh.J., M.Sh., Ye.Zh., Y.Zh.,; resources, X.T.; data curation, X.T.and M.Sh; writing—original draft preparation, X.T., L.Ch., Y.L., Zh.J., M.Sh., Ye.Zh., Y.Zh. ; writing—review and editing, L.Ch.; visualization, X.T., M.Sh and Y.Zh; supervision, L.Ch. and Y.Zh; project administration, L.Ch. and Y.Zh; funding acquisition, Y.Zh and Zh.J .All authors have read and agreed to the published version of the manuscript." Please turn to the CRediT taxonomy for the term explanation. Authorship must be limited to those who have contributed substantially to the work reported.

Acknowledgments

Work by Yu Zheng was supported by the National key R & D Program's plan for strategic international science and technology cooperation and innovation (grant no. 2018YFE0206500) and Systems Science Plus Joint Research Program of Qingdao University (XT2024301). Work by L. F. Chernogor was supported by the National Research Foundation of Ukraine for financial support (project2020.02/0015, «Theoretical and experimental studies of global disturbances from natural and technogenic sources in the Earth-atmosphere-ionosphere system») and Ukraine state-funded research projects #0121U109881 and #0122U001476. We acknowledged the use of data from the Chinese MeridianProject.

Open research

The results presented in this paper rely on data collected at magnetic observatories. We thank the national institutes that support them and INTERMAGNET for promoting high standards of magnetic observatory practice (www.intermagnet.org). The solar wind parameters have been retrieved from the Goddard Space Flight Center Space Physics Data Facility https://omniweb.gsfc.nasa.gov/form/dx1.html. The satellite data were obtained from the Chinese MeridianProject. www.meridianproject.ac.cn.

Declaration of interests

The authors declare no conflicts of interest.

References

Aa, E., Chen, Y., & Luo, B. (2024b). Dynamic expansion and merging of the equatorial ionization anomaly during the 10–11 May 2024 super geomagnetic storm. *Remote Sensing*, *16*(22), 4290.https://doi.org/10.3390/rs16224290

Aa, E., Zhang, S. R., Lei, J., Huang, F., Erickson, P. J., Coster, A. J., ... & Kerr, R. B. (2024a). Significant midlatitude plasma density peaks and dual-hemisphere SED during the 10–11 May 2024 super geomagnetic storm. *Journal of Geophysical Research: Space Physics*, *129*(11), e2024JA033360. https://doi.org/10.1029/2024JA033360

Bojilova, R. (2024, October). First Results for the Influence of Two Geomagnetic Storms during 10-12 May 2024 On Mid-latitude Ionosphere. In *Proceedings of the Bulgarian Academy of Sciences* (Vol. 77, No. 10, pp. 1485-1492).https://doi.org/10.7546/CRABS.2024.10.08

Bojilova, R., Mukhtarov, P., & Pancheva, D. (2024). Global ionospheric response during extreme geomagnetic storm in may 2024. *Remote Sensing*, *16*(21), 4046.https://doi.org/10.3390/rs16214046

Chernyshov, A. A., Klimenko, M. V., Nosikov, I. A., Borchevkina, O. P., Timchenko, A. V., Efishov, I. I., ... & Chugunin, D. V. (2025). Effects in the upper atmosphere and ionosphere in the subauroral region during Victory Day 2024 Geomagnetic Storm (May 10-12, 2024). *Advances in Space Research*. https://doi.org/10.1016/j.asr.2025.02.015

Carmo, C. S., Dai, L., Wrasse, C. M., Barros, D., Takahashi, H., Figueiredo, C. A. O. B., ... & Liu, Z. (2024). Ionospheric response to the extreme 2024 mother's day geomagnetic storm over the Latin American sector. *Space Weather*, *22*(12), e2024SW004054. https://doi.org/10.1029/2024SW004054

Chernogor, L. F. (2003). Physics of Earth, atmosphere, and geospace from the standpoint of system paradigm. *Radio Physics and Radio Astronomy*, *8*, 59.

Chernogor, L. F. (2008). Advanced methods of spectral analysis of quasiperiodic wave-like processes in the ionosphere: Specific features and experimental results. *Geomagnetism and Aeronomy*, *48*(5), 652-673. https://doi.org/10.1134/S0016793208050101

Chernogor, L. F. (2021). Physics of geospace storms. *Space Science and Technology*, *27*(1).https://doi.org/10.15407/knit2021.01.003

Chernogor, L. F. (2025). Energetics of physical processes operated on May 8–12, 2024: From the solar storm to lithospheric disturbances. *Advances in Space Research*.https://doi.org/10.1016/j.asr.2024.12.069

Evans, J. S., Correira, J., Lumpe, J. D., Eastes, R. W., Gan, Q., Laskar, F. I., ... & Veibell, V. (2024). GOLD observations of the thermospheric response to the 10-12 May 2024 geomagnetic storm. *Authorea Preprints*. https://doi.org/10.22541/essoar.171926407.71074494/v1

Foster, J. C., Erickson, P. J., Nishimura, Y., Zhang, S. R., Bush, D. C., Coster, A. J., ... & Franco-Diaz, E. (2024). Imaging the May 2024 extreme aurora with ionospheric total electron content. *Geophysical Research Letters*, *51*(20), e2024GL111981. https://doi.org/10.1029/2024GL111981

Fu, W. D., Fu, H. S., Zhang, W. Z., Yu, Y., & Cao, J. B. (2025). Compression of Earth's magnetopause down to 5 RE during the superstorm on 10 May 2024. *Geophysical Research Letters*, *52*(5), e2024GL114040.https://doi.org/10.1029/2024GL114040

Gonzalez-Esparza, J. A., Sanchez-Garcia, E., Sergeeva, M., Corona-Romero, P., Gonzalez-Mendez, L. X., Valdes-Galicia, J. F., ... & Hernandez-Quintero, E. (2024). The mother's day geomagnetic storm on 10 May 2024: Aurora observations and low latitude space weather effects in Mexico. *Space Weather*, *22*(11), e2024SW004111. https://doi.org/10.1029/2024SW004111

Guo, X., Zhao, B., Yu, T., Hao, H., Sun, W., Wang, G., ... & Ren, Z. (2024). East–west difference in the ionospheric response during the recovery phase of May 2024 super geomagnetic storm over the East Asian. *Journal of Geophysical Research: Space Physics*, *129*(9), e2024JA033170. https://doi.org/10.1029/2024JA033170

Huang, F., Lei, J., Zhang, S. R., Wang, Y., Li, Z., Zhong, J., ... & Luan, X. (2024). Peculiar nighttime ionospheric enhancements over the Asian sector during the May 2024 Superstorm. *Journal of Geophysical Research: Space Physics*, *129*(11), e2024JA033350. https://doi.org/10.1029/2024JA033350

Hajra, R., Tsurutani, B. T., Lakhina, G. S., Lu, Q., & Du, A. (2024). Interplanetary causes and impacts of the 2024 May superstorm on the geosphere: An overview. *The Astrophysical Journal*, *974*(2), 264. https://doi.org/10.3847/1538-4357/ad7462

Hayakawa, H., Ebihara, Y., Mishev, A., Koldobskiy, S., Kusano, K., Bechet, S., ... & Miyoshi, Y. (2025). The Solar and Geomagnetic Storms in 2024 May: A Flash Data Report. *The Astrophysical Journal*, *979*(1), 49.https://doi.org/10.3847/1538-4357/ad9335

Jain, A., Trivedi, R., Jain, S., & Choudhary, R. K. (2025). Effects of the Super Intense Geomagnetic Storm on 10-11 May, 2024 on Total Electron Content at Bhopal. *Advances in Space Research*, *75*(1), 953-965. https://doi.org/10.1016/j.asr.2024.09.029

Jin, Y., Kotova, D., Clausen, L. B., & Miloch, W. J. (2025). Significant plasma density depletion from high-to mid-latitude ionosphere during the super storm in May 2024. *Geophysical Research Letters*, *52*(5), e2024GL113997.https://doi.org/10.1029/2024GL113997

Karan, D. K., Martinis, C. R., Daniell, R. E., Eastes, R. W., Wang, W., McClintock, W. E., ... & England, S. (2024). GOLD observations of the merging of the Southern Crest of the equatorial ionization anomaly and aurora during the 10 and 11 May 2024 Mother's Day super geomagnetic storm. *Geophysical Research Letters*, *51*(15), e2024GL110632. https://doi.org/10.1029/2024GL110632

Kwak, Y. S., Kim, J. H., Kim, S., Miyashita, Y., Yang, T., Park, S. H., ... & Talha, M. (2024). Observational Overview of the May 2024 G5-Level Geomagnetic Storm: From Solar Eruptions to Terrestrial Consequences. *Journal of Astronomy and Space Sciences*, *41*(3), 171-194. https://doi.org/10.5140/JASS.2024.41.3.171

Li, W., Liu, L., Yang, Y., Han, T., Du, R., Zhang, R., ... & Chen, Y. (2024). Interhemispheric and longitudinal differences in the ionosphere–thermosphere coupling process during the May 2024 superstorm. *Earth and Planetary Physics*, *8*(6), 910-919.https://doi.org/10.26464/epp2024073

Myint, L. M., Perwitasari, S., Nishioka, M., Saito, S., Kaewthongrach, R., & Supnithi, P. (2025). Analysis of Ionospheric and Geomagnetic Fields Changes in Thailand During the May 2024 Geomagnetic Storm. *Advances in Space Research*.https://doi.org/10.1016/j.asr.2025.01.071

Mlynczak, M. G., Hunt, L. A., Nowak, N., Marshall, B. T., & Mertens, C. J. (2024). Global thermospheric infrared response to the Mother's day weekend extreme storm of 2024. *Geophysical Research Letters*, *51*(15), e2024GL110701.https://doi.org/10.1029/2024GL110701

Nayak, C., Buchert, S., Yiğit, E., Ankita, M., Singh, S., Tulasi Ram, S., & Dimri, A. P. (2025). Topside low-latitude ionospheric response to the 10–11 May 2024 super geomagnetic storm as observed by Swarm: The strongest storm-time super-fountain during the Swarm era?. *Journal of Geophysical Research: Space Physics*, *130*(3), e2024JA033340.https://doi.org/10.1029/2024JA033340

Paul, K. S., Moses, M., Haralambous, H., & Oikonomou, C. (2025). Effects of the Mother's Day Superstorm (10–11 May 2024) over the Global Ionosphere. *Remote Sensing*, *17*(5), 859.https://doi.org/10.3390/rs17050859

Pierrard, V., Verhulst, T. G., Chevalier, J. M., Bergeot, N., & Winant, A. (2025). Effects of the Geomagnetic Superstorms of 10–11 May 2024 and 7–11 October 2024 on the Ionosphere and Plasmasphere. *Atmosphere*, *16*(3), 299.https://doi.org/10.3390/atmos16030299

Pierrard, V., Winant, A., Botek, E., & Péters de Bonhome, M. (2024). The Mother's Day Solar Storm of 11 May 2024 and Its Effect on Earth's Radiation Belts. *Universe*, *10*(10), 391. https://doi.org/10.3390/universe10100391

Ranjan, A. K., Nailwal, D., Sunil Krishna, M. V., Kumar, A., & Sarkhel, S. (2024). Evidence of potential thermospheric overcooling during the May 2024 geomagnetic superstorm. *Journal of Geophysical Research: Space Physics*, *129*(12), e2024JA033148. https://doi.org/10.1029/2024JA033148

Rout, D., Kumar, A., Singh, R., Patra, S., Karan, D. K., Chakraborty, S., ... & Riccobono, J. (2025). Evidence of unusually strong equatorial ionization anomaly at three local time sectors during the mother's day geomagnetic storm on 10–11 May 2024. *Geophysical Research Letters*, *52*(2), e2024GL111269.https://doi.org/10.1029/2024GL111269

Rodkin, D., Lukmanov, V., Slemzin, V., & Chashei, I. (2024). Observation and modeling of complex transient structure in heliosphere followed by geomagnetic storm on May 10–11, 2024. *Advances in Space Research*.https://doi.org/10.1016/j.asr.2024.12.068

Resende, L. C. A., Zhu, Y., Santos, A. M., Chagas, R. A. J., Denardini, C. M., Arras, C., ... & Liu, Z. (2024). Nocturnal Sporadic Cusp-Type Layer (Esc) Resulting From Anomalous Excess Ionization Over the SAMA Region During the Extreme Magnetic Storm on 11 May 2024. *Journal of Geophysical Research: Space Physics*, *129*(11), e2024JA033167.https://doi.org/10.1029/2024JA033167

Shi, Y. F., Yang, C., Wang, J., Zheng, Y., Meng, F. Y., & Chernogor, L. F. (2023). A hybrid deep learning-based forecasting model for the peak height of ionospheric F2 layer. *Space Weather*, *21*(10), e2023SW003581. https://doi.org/10.1029/2023sw003581

Shi, Y., Yang, C., Wang, J., Zhang, Z., Meng, F., & Bai, H. (2023). A forecasting model of ionospheric foF2 using the LSTM network based on ICEEMDAN decomposition. *IEEE Transactions on Geoscience and Remote Sensing*, *61*, 1-16. https://doi.org/10.1109/tgrs.2023.3336934

Singh, R., Scipión, D. E., Kuyeng, K., Condor, P., De La Jara, C., Velasquez, J. P., ... & Migliozzi, M. (2024). Ionospheric disturbances observed over the Peruvian sector during the Mother's Day Storm (G5-level) on 10–12 May 2024. *Journal of Geophysical Research: Space Physics*, *129*(11), e2024JA033003.https://doi.org/10.1029/2024JA033003

Sun, W., Li, G., Zhao, B., Zhang, S. R., Otsuka, Y., Hu, L., ... & Perwitasari, S. (2024a). Midlatitude plasma blob-like structures along with super equatorial plasma bubbles during the May 2024 great geomagnetic storm. *Geophysical Research Letters*, *51*(21), e2024GL111638. https://doi.org/10.1029/2024GL111638

Sun, W., Li, G., Zhang, S. R., Zhao, B., Li, Y., Tariq, M. A., ... & Liu, L. (2024b). Complex ionospheric fluctuations over East and Southeast Asia during the May 2024 super geomagnetic storm. *Journal of Geophysical Research: Space Physics*, *129*(12), e2024JA033096. https://doi.org/10.1029/2024JA033096

Shi, Y., Yang, C., Wang, J., & Meng, F. (2025). A hybrid deep learning-based short-term forecast model for ionospheric foF2 in East Asia region. *Advances in Space Research*, *75*(1), 988-1002. https://doi.org/10.1016/j.asr.2024.09.062

Themens, D. R., Elvidge, S., McCaffrey, A., Jayachandran, P., Coster, A., Varney, R. H., ... & Reid, B. (2024). The high latitude ionospheric response to the major May 2024 geomagnetic storm: A synoptic view. *Geophysical Research Letters*, *51*(19), e2024GL111677. https://doi.org/10.1029/2024GL111677

Tulasi Ram, S., Veenadhari, B., Dimri, A. P., Bulusu, J., Bagiya, M., Gurubaran, S., ... & Vichare, G. (2024). Super-intense geomagnetic storm on 10–11 May 2024: Possible mechanisms and impacts. *Space Weather*, *22*(12), e2024SW004126. https://doi.org/10.1029/2024SW004126

Thampi, S. V., Venugopal, I., & Bhaskar, A. T. (2024). Super-fountain Effect: Unleashing the Role of Electric Fields During the Extreme Geomagnetic Storm on May 10-11, 2024. *Authorea Preprints*. https://doi.org/10.22541/essoar.172434426.60233888/v1

Vichare, G., & Bagiya, M. S. (2024). Manifestations of strong IMF-by on the equatorial ionospheric electrodynamics during 10 May 2024 geomagnetic storm. *Geophysical Research Letters*, *51*(23), e2024GL112569.https://doi.org/10.1029/2024GL112569

Wang, H., Cheng, Q., Lühr, H., Zhong, Y., Zhang, K., & Xia, H. (2024). Local time and hemispheric asymmetries of field-aligned currents and polar electrojet during May 2024 superstorm periods. *Journal of Geophysical Research: Space Physics*, *129*(11), e2024JA033020. https://doi.org/10.1029/2024JA033020

Wang, J., Feng, F., & Ma, J. (2020). An adaptive forecasting method for ionospheric critical frequency of F2 layer. *Radio Science*, *55*(1), 1-12 https://doi.org/10.1029/2019rs007001

Wang, R., Liu, Y. D., Zhao, X., & Hu, H. (2024). Unveiling key factors in solar eruptions leading to the solar superstorm in 2024 May. *Astronomy & Astrophysics*, *692*, A112. https://doi.org/10.1051/0004-6361/202452008

Wang, S.,Quan, L., Li, L., Wang, K.,Huang, J., & Yuan, G. (2019). Analysis of the impact and effects of the solar storm on the ionosphere from may 8 to 16, 2024. GNSS World of China, 44(3), 38-48.https://doi.org/10.12265/j.gnss.2024107

Zhang, K., Wang, H., Liu, J., Song, H., & Xia, H. (2025). The quasi-periodic nighttime traveling ionospheric disturbances on 13 May 2024 during the recovery phase of a SuperStorm. *Journal of Geophysical Research: Space Physics*, *130*(1), e2024JA033257.https://doi.org/10.1029/2024JA033257

Zhao, M. X., & Le, G. M. (2025). Dependence of SYMH Change Rate on Dynamic Pressure during the Main Phases of Storms: A Comparative Analysis of the 2024 May and 2003 November Superstorms. *The Astrophysical Journal*, *978*(2), 157.https://doi.org/10.3847/1538-4357/ada15c

Zhang, R., Liu, L., Yang, Y., Li, W., Zhao, X., Yoshikawa, A., ... & Le, H. (2024). Ionosphere responses over Asian-Australian and American sectors to the 10–12 May 2024 superstorm. *Journal of Geophysical Research: Space Physics*, *129*(12), e2024JA033071. https://doi.org/10.1029/2024JA033071